Supplemental material for: "Three-dimensional nuclear spin positioning using coherent radio-frequency control"

J. Zopes[†], K. Herb[†], K. S. Cujia[†], C. L. Degen[*]

[1]*Department of Physics, ETH Zurich, Otto Stern Weg 1, 8093 Zurich, Switzerland.*

I. DIAMOND SAMPLES

The measurements at low magnetic field ($\sim 10\,\mathrm{mT}$) were performed on a bulk, electronic-grade diamond crystal from Element Six. The diamond was overgrown with a layer structure of 20 nm enriched ^{12}C (99.99 %), 1 nm enriched ^{13}C and a 5 nm cap layer of again enriched ^{12}C. Nitrogen-vacancy (NV) centers were generated by ion-implantation of ^{15}N with an energy of 5 keV, corresponding to a depth of $5 - 10\,\mathrm{nm}$. The intrinsic nuclear spin of the two NV centers studied in our experiments were confirmed to be of the ^{15}N isotope. Further characterizations and details on the sample can be found in a recent study (sample B in Ref. [1]).

The measurements at high magnetic field ($\sim 205\,\mathrm{mT}$) were performed on an electronic-grade, natural abundance (1.1 % ^{13}C) diamond membrane. Nitrogen-vacancy (NV) centers were again generated by ion-implantation of ^{15}N with an energy of 5 keV. We etched nano-pillars into the diamond surface to increase the photon collection efficiency.

II. NUCLEAR SPIN INITIALIZATION

We transferred polarization from the optically polarized NV center to the target nuclear spin using the pulse sequence shown in Fig. S1 (a). The sequence has been introduced by Taminiau *et al.* in Ref. [2] and acts as an effective swap gate between electron and nuclear spins. It requires only microwave and laser pulses to be applied to the NV center. Controlled X-rotations rotate the nuclear spin around the $\pm X$-direction dependent on the m_S-state of the NV center and are implemented by a Carr-Purcell (CP) sequence of microwave pulses in analogy with the hyperfine-mediated $\pi/2$-rotation discussed in the main text. The interpulse delay τ is resonant with the precession frequency of the nuclear spin. The final optical reinitialization of the NV center with

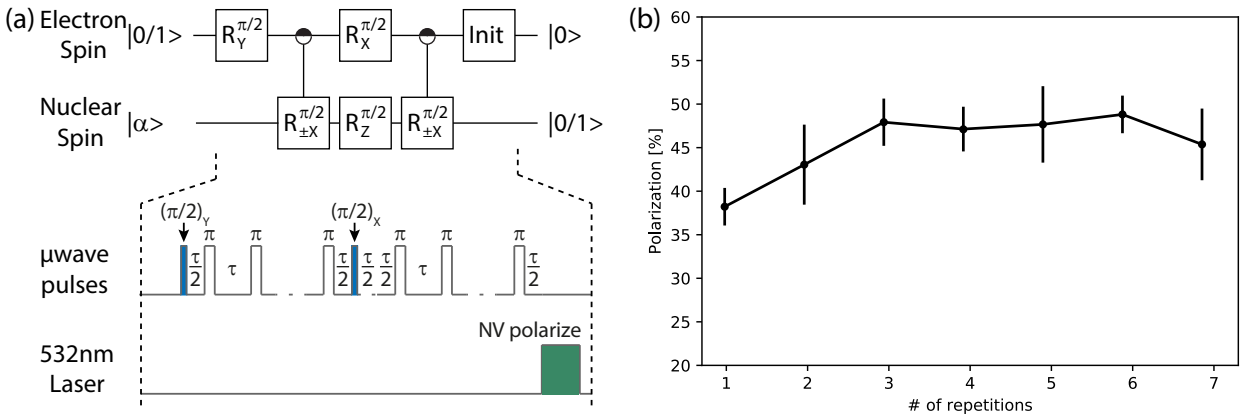

FIG. S1: Nuclear spin initialization. (a) Nuclear spin polarization protocol for a single ^{13}C nuclear spin as devised in Ref. [2]. The upper part of the schematic illustrates the sequence in the framework of controlled single and two-qubit gates. The external control of the spin system is realized by microwave and laser pulses applied to the NV center and the experimental realization is shown in the lower part of the schematic. The interpulse delay τ is held fixed and resonant to the precession frequency of the target nuclear spin. (b) Polarization build-up of an individual nuclear spin after repeated application of the sequence shown in (a).

a short laser pulse (duration $\sim 2\,\mu$s, indicated in green in Fig. S1 (a)) preserves the nuclear spin polarization.

The build-up of the nuclear spin polarization after repetitive application of the protocol is shown in Fig. S1 (b). Here, the polarization is detected by quantum state tomography of the nuclear I_z expectation value after N applications of the polarization sequence. We note that nuclei can also be polarized by other dynamic nuclear polariziation (DNP) methods like nuclear orientation via electron spin locking (NOVEL, [3]) or cross-relaxation induced polarization (CRIP, [4]).

III. CALIBRATION OF RADIO-FREQUENCY PULSES VIA SNAPSHOT ODMR

As discussed in the main text, we calibrate the temporal shape of the radio-frequency pulses by performing two-dimensional electron spin resonance experiments. The applied pulse sequence is shown in Fig. S2 and will be described in the following in conjunction with the typical experimental parameters: Initially the NV center is polarized in the $m_S = 0$ state with a short optical pulse (duration $\sim 2\,\mu$s). Subsequently we apply the rf-pulse to the coil circuit and a microwave pulse

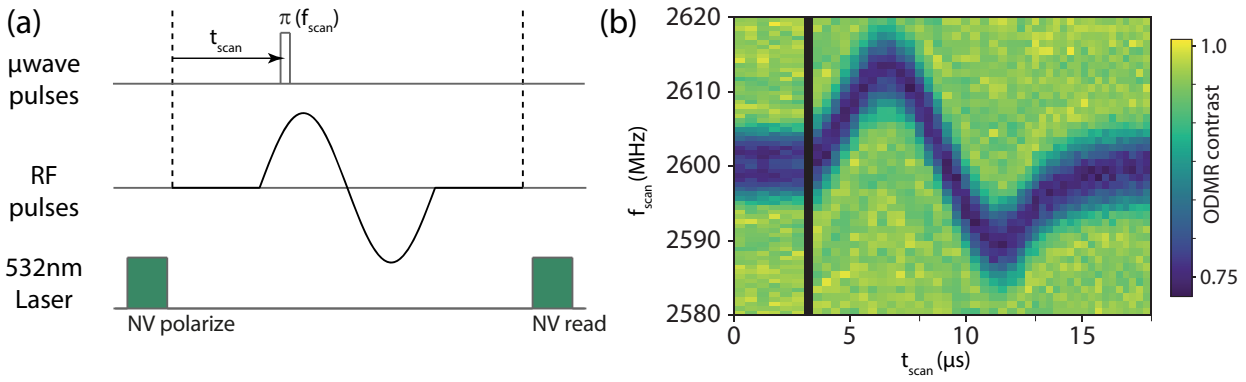

FIG. S2: (a) Pulse sequence for the two-dimensional, snapshot ODMR technique used to calibrate the temporal shape of the radio-frequency pulses generated by the coil. (b) Resulting two-dimensional ODMR spectrum reproduced from Fig. 2 (b) in the main text and with axes relabeled to t_{scan} and f_{scan} as defined in (a).

with variable frequency (f_{scan}) and relative time delay (t_{scan}) to the NV center. The control signals are generated by two arbitrary waveform generators, which are locked to the same reference clock and whose signal generation is started upon a shared trigger pulse. After applying both pulses, the NV center is readout with a second laser pulse. As the parallel projection of the coil magnetic field detunes the NV center's EPR transition, the detection of this detuning enables us to determine the temporal shape of the rf-pulse. The duration of the microwave pulse was typically 100 ns and calibrated to perform a π rotation on resonance. We stepped the relative timing t_{scan} in increments of $100-400$ ns and swept the frequency (f_{scan}) in steps of $0.5-1$ MHz over a bandwidth of ~ 50 MHz. The amplitude of the radio-frequency pulses was typically reduced during the calibration procedure to prevent excessive heating as the duty cycle during calibration is significantly higher than during the azimuthal positioning measurements.

IV. DENSITY MATRIX SIMULATIONS AND ESTIMATION OF ϕ

We performed density matrix simulations for all measurements and extracted the nuclear azimuthal location ϕ using non-linear least squares fitting [5]. We used the Quantum Toolbox in Python (QuTiP, [6]) software package to set up spin operators and compute the time-evolution propagators. We propagate the initial density matrix $\rho = |0\rangle\langle 0| \otimes I_e/2$ using time-independent Hamiltonians through the full measurement sequence, including the nuclear polarization step. Here

$|0\rangle\langle 0|$ is the projector on the $m_s = 0$ state of the NV center and I_e is the nuclear spin identity. All timings are taken from the pulse file that was uploaded to the arbitrary waveform generators (AWG) controlling the experiments. Further input parameters are the parallel and perpendicular hyperfine parameters $(a_{||}, a_{\perp})$, calibrated by conventional correlation spectroscopy [7], as well as the magnetic vector orientation and temporal shape of the coil rf pulse.

We reconstruct the azimuthal angle ϕ in two consecutive steps from the measurements: First, we determine the precession frequency of the nuclear spin. The precession frequency is a critical parameter in our experiments, because uncertainty in the frequency directly translates into an uncertainty in the detected phases and thereby to an uncertainty in the azimuthal position ϕ. We estimate the nuclear precession frequency using the reference measurement traces, which were acquired after rotating the nuclear spin via the hyperfine interaction. The most precise estimate of the precession frequency can be obtained by simulating the dynamics of the nuclear-electron spin system to include the coherent evolution of the nuclear spin starting from the rotation with the NV center until the read-out of the NV center. The total evolution or interrogation time in our experiments is typically $20 - 40\,\mu$s long and therefore the precession frequency of the nuclear spin can be determined very precisely.

We fit the simulation to the reference measurement with the magnitude of the external bias field B_0 as a free parameter to adjust the precession frequency. Here, the bias field is assumed to be aligned with the symmetry axis of the NV center. A discussion of the effect of tilted magnetic fields follows in Section V. We fit the simulated time trace to the experimental data with a non-linear least-squares optimization. Apart from the bias field B_0 we only allow for an amplitude scaling factor (accounting for non-ideal nuclear polarization, *e.g.* , due to relaxation) plus a constant offset as additional free parameters of the fit. Using this procedure, we determine B_0 with an uncertainty smaller than $\delta B_0 = 10\,\mu$T, which corresponds to an uncertainty of the nuclear precession frequency of $\sim 100\,$Hz.

Afterwards, we determine the azimuthal position of the nuclear spin using the nuclear precession trace after a rotation with the micro-coil. Again, we simulate the dynamics of the spin system by propagating the density matrix with B_0 now fixed. The temporal shape of the coil pulse, as determined by the 2D spectroscopy, and the vector field of the coil are added as input parameters to the simulation. The evolution of the nuclear spin during the rf-pulse is approximated by piecewise constant propagators during which the Hamiltonian is time-independent. We operate in the non-

rotating reference frame of the nuclear spin, hence counter-rotating terms leading, *e.g.* , to the Bloch-Siegert shift are also captured by the simulation. Again we use a non-linear least squares optimization procedure to fit the simulated time trace to the experimental data. The free parameters are the nuclear azimuthal position ϕ and an offset and an amplitude scaling factor.

V. EFFECT OF TILTED MAGNETIC BIAS FIELDS ON THE ACCURACY IN ESTIMATING $\vec{r} = (r, \theta, \phi)$

As discussed in the main text we have carefully aligned the magnetic bias field B_0 to the quantization axis of the NV center with a resulting tilt smaller than $1\,^\circ$. Here, we discuss the influence of the residual tilt on the accuracy in estimating the nuclear position.

We performed a detailed analysis of the positioning accuracy by making use of the density matrix simulations (Section IV) to perform a Monte Carlo sampling of the distribution of the estimates (r, θ, ϕ). As an example, we consider nuclear spin $^{13}C_3$, whose three-dimensional position was determined in a magnetic field of $B_0 = 204.902(9)\,\mathrm{mT}$. All other nuclear spins were positioned in a significantly smaller magnetic field of $9.600(8)$ mT, where the alignment of the magnetic field can be performed much more precisely using auxiliary calibration NV centers, as described in [8]. Hence, the positioning uncertainty due to tilted magnetic fields is significantly smaller in low magnetic field (approximately one order of magnitude) and $^{13}C_3$ serves as a worst-case estimate.

The error estimation protocol follows a two-step process: First, we generate artificial measurement data with a random field tilt and a given nuclear positon (r, θ, ϕ). In a second step, we use the procedures described in Section IV to estimate $(\tilde{r}, \tilde{\theta}, \tilde{\phi})$. Finally, we compare the resulting values to the input coordinates. In each iteration of this Monte Carlo (MC) simulation we add random transverse magnetic field components which were drawn from a normal distribution with mean zero and standard deviation $\sigma = 1.4\,\mathrm{mT}$. This corresponds to tilts of $\sim 1\,^\circ$. In the resulting tilted magnetic field we simulated each step of the three-dimensional positioning protocol. First, we simulated the outcome of correlation spectroscopy experiments [7] to infer $(\omega_L, a_{||}, a_\perp)$. From these parameters, we directly obtain the estimates of (r, θ) of the nuclear spin location by inverting the relations for $(a_{||}, a_\perp)$ [8]. Due to the tilt of the magnetic field the hyperfine coupling parameters are slightly modified, which leads to a distribution of (r, θ) which depends on (B_x, B_y). These distributions are shown as histograms in Fig. S3 (a,b), respectively. The resulting variations in r

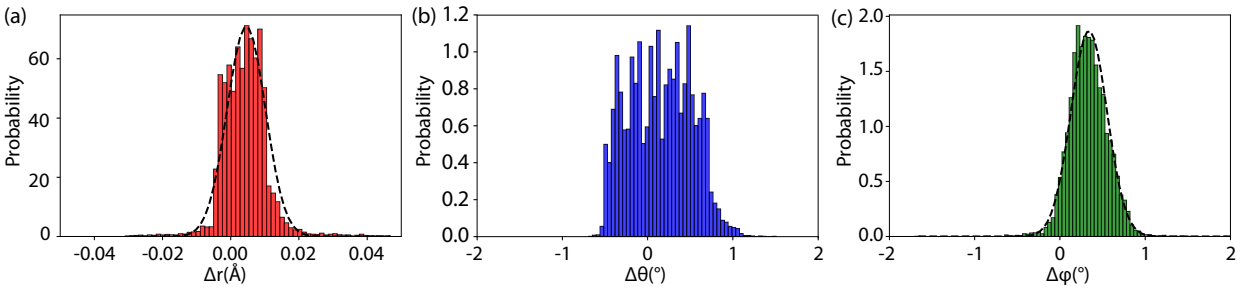

FIG. S3: Nuclear positioning uncertainty due to tilted bias fields for $^{13}C_3$. (a) Histogram of the distribution of deviations in the estimated radial distance Δr from the actual distance r. The histogram contains 10949 samples of a Monte Carlo simulation described in the text. (b) Histogram of the deviation of θ obtained from the same Monte Carlo simulation as in (a) and with the same sample size. (c) Histogram of the deviation in ϕ. The average tilt in the Monte Carlo simulation generating the distribution was set to $\sim 1°$.

and θ amounts to $\sim 0.01\,\text{Å}$ and $\sim 0.5\,°$, respectively. For the histograms we generated 19140 Monte Carlo samples. Afterwards, we post-selected $N = 10949$ samples for which the deviation between nuclear precession frequency, obtained from the simulated correlation spectroscopy, and the one predicted by the EPR frequency (by diagonalizing the Hamiltonian) is smaller than $2\pi \times 1\,\text{kHz}$. This condition was enforced in all experiments.

Subsequently, we simulate the azimuthal imaging protocol as discussed before. The interpulse spacing τ of the multipulse sequences used for the AC magnetometry was adjusted based on the result of the correlation spectroscopy. The outcome of the simulation, *i.e.* , the precession trace of the nuclear spin is analyzed by the non-linear fitting procedure (see Section IV), in the same manner as the experimental traces. The resulting distribution of $\Delta\phi$ is shown in Fig. S3 (c). We find that the variation in $\Delta\phi$ amounts to $\sim 0.3\,°$. The distributions of $(\Delta r, \Delta\theta, \Delta\phi)$ are not exactly centered at zero because of the gyromagnetic ratio enhancement of the nuclear spin resulting from the transverse magnetic fields [9].

[1] T. Unden, N. Tomek, T. Weggler, F. Frank, P. London, J. Zopes, C. L. Degen, N. Raatz, J. Meijer, H. Watanabe, et al., npj Quantum Information **4**, 39 (2018), URL https://doi.org/10.1038/s41534-018-0089-8.

[2] T. H. Taminiau, J. Cramer, T. van der Sar, V. V. Dobrovitski, and R. Hanson, Nature Nano. **9**, 171 (2014).

[3] P. London, J. Scheuer, J. M. Cai, I. Schwarz, A. Retzker, M. B. Plenio, M. Katagiri, T. Teraji, S. Koizumi, J. Isoya, et al., Phys. Rev. Lett. **111**, 067601 (2013).

[4] D. A. Broadway, J. P. Tetienne, A. Stacey, J. A. Wood, D. A. Simpson, L. T. Hall, and L. C. L. Hollenberg, Nature Communications **9**, 1246 (2018).

[5] M. Newville, T. Stensitzki, D. B. Allen, and A. Ingargiola, *LMFIT: Non-Linear Least-Square Minimization and Curve-Fitting for Python* (2014), URL https://doi.org/10.5281/zenodo.11813.

[6] J. Johansson, P. Nation, and F. Nori, Computer Physics Communications **184**, 1234 (2013), ISSN 0010-4655.

[7] J. M. Boss, K. Chang, J. Armijo, K. Cujia, T. Rosskopf, J. R. Maze, and C. L. Degen, Phys. Rev. Lett. **116**, 197601 (2016).

[8] J. Zopes, K. S. Cujia, K. Sasaki, J. M. Boss, K. M. Itoh, and C. L. Degen, arXiv:1806.04883 (2018), URL https://arxiv.org/abs/1806.04883.

[9] L. Childress, M. V. G. Dutt, J. M. Taylor, A. S. Zibrov, F. Jelezko, J. Wrachtrup, P. R. Hemmer, and M. D. Lukin, Science **314**, 281 (2006), URL http://dx.doi.org/10.1126/science.1131871.